Available online at www.sciencedirect.com

SciVerse ScienceDirect

Ceramics International 38 (2012) 4561–4571

CERAMICS INTERNATIONAL

www.elsevier.com/locate/ceramint

Microwave absorption study of carbon nano tubes dispersed hard/soft ferrite nanocomposite

Sachin Tyagi [a,*], Palash Verma [a], Himanshu B. Baskey [b], Ramesh Chandra Agarwala [a], Vijaya Agarwala [a], Trilok Chand Shami [b]

[a] *Surface Engineering Lab, Department of Metallurgical and Materials Engineering, Indian Institute of Technology, Roorkee 247667, India*
[b] *Special Materials Group, DMSRDE (DRDO Lab) Kanpur, (Uttar Pradesh), India*

Received 4 May 2011; received in revised form 8 February 2012; accepted 13 February 2012
Available online 8 March 2012

Abstract

Nickel substituted strontium hexaferrite, $SrNi_2Fe_{10}O_{19}$·($SrFe_{12}O_{19}$/$NiFe_2O_4$) nanoparticles have been synthesized by low combustion method by citrate precursors using sol to gel (S–G) followed by gel to nano crystalline (G–N) conversion. The resulting 'as-synthesized' powder is heat treated (HT) at 800 and 1000 °C for 4 h in nitrogen atmosphere. The hysteresis loops show an increase in saturation magnetization from 27.443 to 63.706 emu/g with increasing HT temperatures. The multiwalled carbon nano tubes (CNTs) were synthesized by thermal decomposition of acetylene gas over iron-catalyst deposited on silicon wafer in the temperature range of 750–800 °C. A microwave absorbing medium is prepared by adding CNTs in the nickel substituted strontium hexaferrite nanoparticles. Addition of certain mass of CNTs improves the microwave absorption properties and wave band of $SrFe_{12}O_{19}$/$NiFe_2O_4$ absorbent. When 10 wt% CNTs is mixed with $SrFe_{12}O_{19}$/$NiFe_2O_4$ nanoparticles to fabricate a composite with 2 mm thickness, the maximum reflection loss reaches to −36.817 dB at 9.292 GHz and −10 dB bandwidth reaches 3.27 GHz.

Keywords: A. Sol–gel processes; B. Composites; C. Dielectric properties

1. Introduction

Recently, electromagnetic interference (EMI) problems have been attracting considerable attention due to the extensive use of electromagnetic (EM) waves in wireless communications. EM waves of 0.8–1.2 GHz are used for mobile phones, 2.45 GHz for electronic ranges, 5.6–8.2 GHz (G-band) for synthetic aperture radar (SAR) or microwave communication on the ground, 8.2–12.4 GHz (X-band) and 12.4–18 (Ku-band) for SAR or electron spin resonance (ESR) apparatus [1]. The research pursuing to the development of various EM wave absorbers has been given much attention. Single material like barium hexaferrite [2], strontium hexaferrite [3,4], calcium hexaferrite [5], nickel ferrite [6], zinc ferrite [7], cobalt ferrite [8] or materials contain carbon (charcoal, carbon black, graphite or carbon nano tubes) [9,10] alone cannot meet the demand of large absorption peak, wide working frequency range and thin absorption layer. In order to improve electromagnetic absorption properties, new systems have been evolved comprising of composite powder including carbon powder/silicon carbide [11], earth–iron–boron [12], (Ni–P)/$BaNi_{0.4}Ti_{0.4}Fe_{11.2}O_{19}$ [13], Fe/Z type ferrite [14], Co/CNTs [15], ZnO/CNTs [16] and hard/soft ferrite nanocomposite [17] etc. Since EM wave absorption property of composite depend on electric (complex permittivity) and magnetic (complex permeability) properties of material. The electric loss of composite depends on ohmic and polarization loss of energy, which can be obtained by adding losing fillers like carbon black, graphite, CNTs or carbon fiber to a matrix [18,19]. The magnetic loss depends on big hysteresis attenuation, which can be obtained when magnetic material like hexaferrite or spinel ferrite or a mixture of hard/soft ferrite is added to a matrix [20].

M type strontium hexaferrite ($SrFe_{12}O_{19}$), which is a hard hexagonal magnetic material, has been a subject of continuous interest for several decades due to its applicability in electronic components, magnetic memories and recording media [21]. The practical application of strontium hexaferrite as a permanent

* Corresponding author. Tel.: +91 01332 285739; fax: +91 01332 285243.
E-mail addresses: matsachin@gmail.com, tyagidmt@iitr.ernet.in (S. Tyagi).

0272-8842/$36.00
doi:10.1016/j.ceramint.2012.02.034

magnet is well known and it is also used as a dielectric or magnetic filler in the electromagnetic filler attenuation materials (EAM). Nickel ferrite ($NiFe_2O_4$) having a cubic spinel structure is a soft magnetic material and is widely studied as microwave absorbing material [6,7]. CNTs as conductive fillers have been studied as microwave absorbing materials [15,16] due to their unique physical, chemical, electrical and mechanical properties like high strength, stiffness, large aspect ratio and low density.

The conventional way of synthesizing hexaferrites involves solid state reaction route having high HT temperature (≥1200 ?C), which results in powders with large particle size, limited chemical homogeneity and low sinterability [22]. So, the preparation of fine and uniform hexaferrite powder without impurity is a challenging task. There are several other processing routes available in the literature [22–26]. Hydrothermal method employs expensive autoclaves, good quality seeds of a fair size and the impossibility of observing the crystal as it grows [27]. Sonochemical synthesis can generate a transient localized hot zone with extremely high temperature gradient and pressure [28] which can assist the destruction of the sonochemical precursor and the formation of nanoparticles. Modified flux method involving co-precipitation of chloride salt by NaOH needs multiple time washing to remove the impurity like NaCl [3,13,17]. Mechanical alloying leads to impurity and lattice strains during milling [22]. The present investigation deals with the synthesis of nickel substituted strontium hexaferrite nanoparticles by low combustion synthesis method. This method is a solution combustion process with higher composition homogeneity and lower flame temperature. The low combustion exothermic reaction accompanied by evolution of large amount of gases results in voluminous and foamy powders with soft agglomeration and large specific area [26]. This method is economical, quite suitable for the synthesis of highly homogenous and active nanosize powder at lower temperature as compared to other methods [3,17,26]. For the growth of carbon nanotubes on substrates, CVD is uniquely superior to other carbon nanotube production technique like arch-discharge and laser-ablation. In these techniques, CNTs have to be produced separately, purified and then manipulated onto the substrates for producing the device. In a CVD system, the growth of carbon nanotube occurs through catalytic decomposition [29] of carbon source gas over nanoparticles of catalyst metal. The quality of grown carbon nanotube depends on the substrate, catalyst used and growth parameter.

In the present paper, the synthesis of multi walled carbon nanotubes on highly doped silicon substrate, deposited with Fe catalyst is studied. Further studies on relative complex permittivity and permeability of ferrite/CNTs composite and their influence on microwave absorption properties are also carried out.

2. Experimental procedure

2.1. Synthesis of hard/soft ferrite

M-type nickel substituted strontium hexaferrite nanoparticles were synthesized by low combustion synthesis method by citrate precursors using sol to gel (S–G) followed by gel to nanocrystalline (G–N) conversion. Stoichiometric amount of metal nitrates ($Fe(NO_3)_3{\cdot}9H_2O$ and $Ni(NO_3)_2{\cdot}6H_2O$) were dissolved completely into deionized water to make an aqueous solution (I), strontium carbonate was dissolved into minimum amount of acetic acid to make another transparent solution (II). Both the above solutions (I) and (II) were mixed with citric acid in a 1:1 molar ratio. The pH of the solution was increased to 7 by addition of ammonia solution. The resulting sol was heated at constant temperature of 80 °C on magnetic stirrer to complete the reaction to form strontium nickel iron citrate precursor. The mixed solution (I+II) was evaporated very slowly over a period of 5 h to dryness. As soon as the solvent removal was completed, dried precursor undergoes a self ignition reaction to form a very fine brown foamy powder of nanocrystalline ferrite. The combustion reaction can be described as follows:

$$SrCO_3 + 2Ni(NO_3)_2{\bullet}6H_2O + 10Fe(NO_3)_3{\bullet}9H_2O + C_6H_8O_7{\bullet}H_2O \downarrow SrNi_2Fe_{10}O_{19} + CO_2 + NO$$

The flow chart of process and various stages during low combustion synthesis method showing S–G followed by G–N conversion of nanocrystalline ferrite are shown in Figs. 1 and 2 respectively.

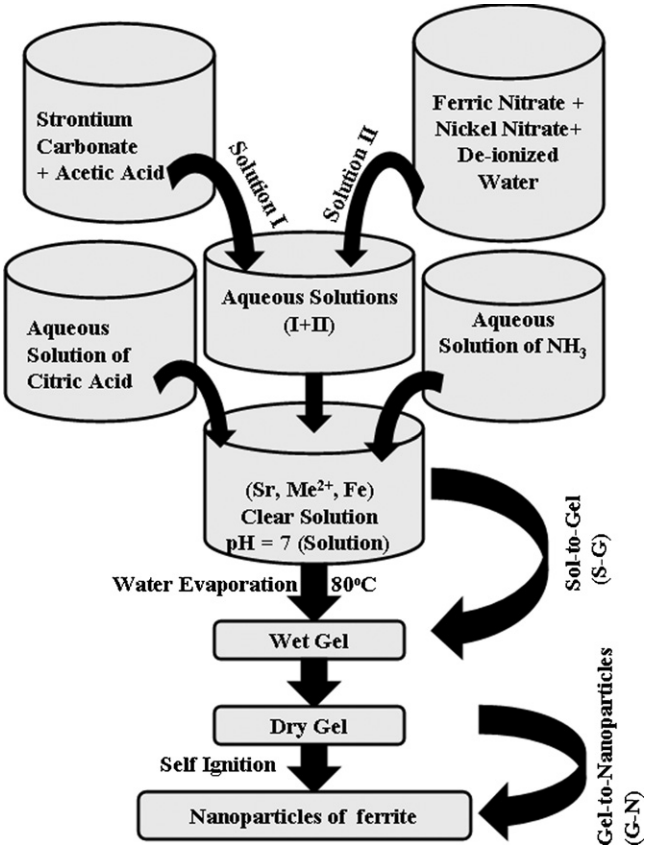

Fig. 1. Flow chart showing the synthesis of $SrFe_{12}O_{19}/NiFe_2O_4$ nanoparticles by low combustion method.

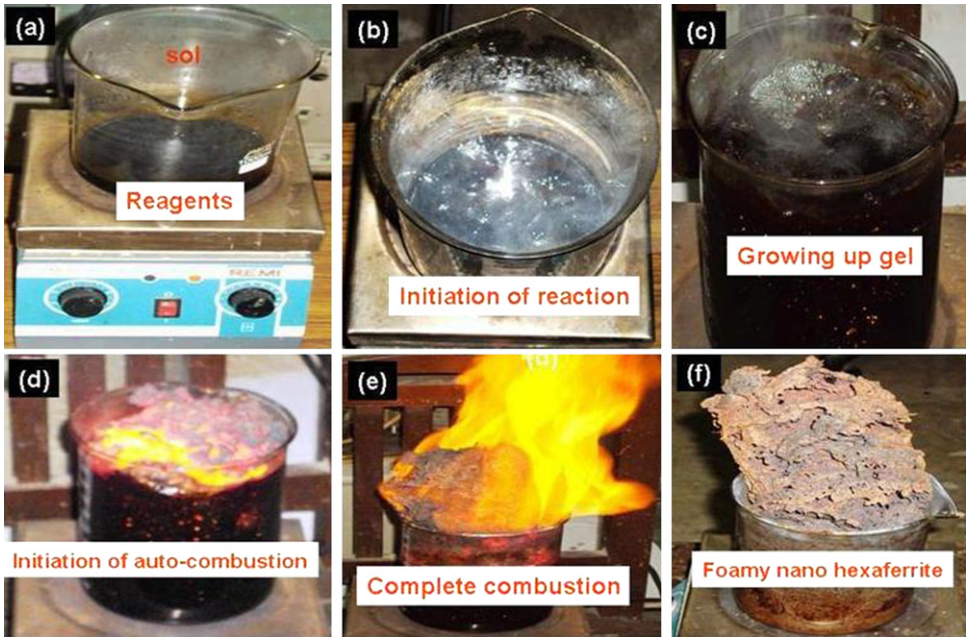

Fig. 2. Photograph showing the various stages of nucleation and growth of $SrFe_{12}O_{19}/NiFe_2O_4$ nanoparticles during synthesis by low combustion method.

2.2. Synthesis of CNTs

The multi walled CNTs were grown over the Si-wafer in a CVD system. The CVD system consists of quartz reactor tube, heated in a resistive tubular furnace, with a substrate positioned in the middle of tubular furnace. The carbon source gas (acetylene) enters the reactor tube directly above the substrate, while the purging and reducing gases enter from both ends of the tube.

The Si-wafer deposited with iron catalyst film is placed in the middle of the quartz tube. The sample is heated upto 700 °C under argon atmosphere. After 750 °C, reducing gas ammonia is introduced, and further flow of argon is stopped. Thermal annealing of iron catalyst film occurs in the temperature range of 750–800 °C under reducing atmosphere, to break it into nanosized particles. Then acetylene gas is introduced, which undergoes catalytic decomposition and the growth of carbon nanotubes occurs over the catalyst nanoparticles. At the end of carbon nanotubes growth period (30 min), argon gas is commenced again; the flow of other gases is stopped. The reactor is cooled down to room temperature, under the flow of argon gas.

3. Characterization studies

Phase identification of annealed ferrite samples and CNTs were done by X-ray diffraction (XRD) using Bruker AXS D8 differactometer with Cu-Kα radiation. The average crystallite size of the ferrite powder was measured by X-ray line broadening technique employing Scherrer's formula. Morphological study was carried out by field emission scanning electron microscope, FESEM (QUANTA FEG 200 FEI) and transmission electron microscope, TEM (Philips, EM 400; TECHNAI 20G2-S-TWIN). Magnetic measurements of ferrite were taken out at room temperature in the applied field range of −10000 to +10000 gauss using vibrating sample magnetometer, VSM (155, PAR). To study the reflection loss properties, the ferrite/CNTs (80 wt%) were mixed with epoxy resin (18 wt%) and hardener (2 wt%). The ferrite/CNTs/epoxy composite thus obtained is cast into a rectangular pellet of thickness 2.0 mm and cured at 75 °C for 30 min. The composite thus prepared is polished and mounted on an aluminum foil (to obtain a single layer metal-backed absorber) to exactly fit into the measuring wave guide. The complex permittivity and permeability measurements were carried out on Network Analyzer (Agilent E8364B PNA series) using material measurement software 85071 in the frequency range of 8.2–12.2 GHz at room temperature. The reflection loss curves were calculated from complex permittivity and permeability at given frequency and absorber thickness with following equations:

$$Z_{in} = Z_0 \left(\frac{\mu_r}{\varepsilon_r}\right)^{1/2} \tanh\left\{ j\frac{2\pi fd}{c}(\mu_r\varepsilon_r)^{1/2} \right\}$$

$$RL = 20\log\left|\frac{Z_{in} - Z_0}{Z_{in} + Z_0}\right|$$

where f is frequency, d is the thickness of absorber (d = 2.0 mm), c is the velocity of light, Z_{in} is the characteristic impedance of absorber and Z_0 is the characteristic impedance in a vacuum, $Z_0 = 120\,\pi$. The impedance matching condition is given by $Z_{in} = Z_0$ to represent the perfect absorbing properties.

4. Results and discussion

The indexed XRD patterns of the $SrFe_{12}O_{19}/NiFe_2O_4$ nanoparticles in 'as synthesized' and after heat treatment at 800 and 1000 °C for 4 h in the nitrogen atmosphere are shown

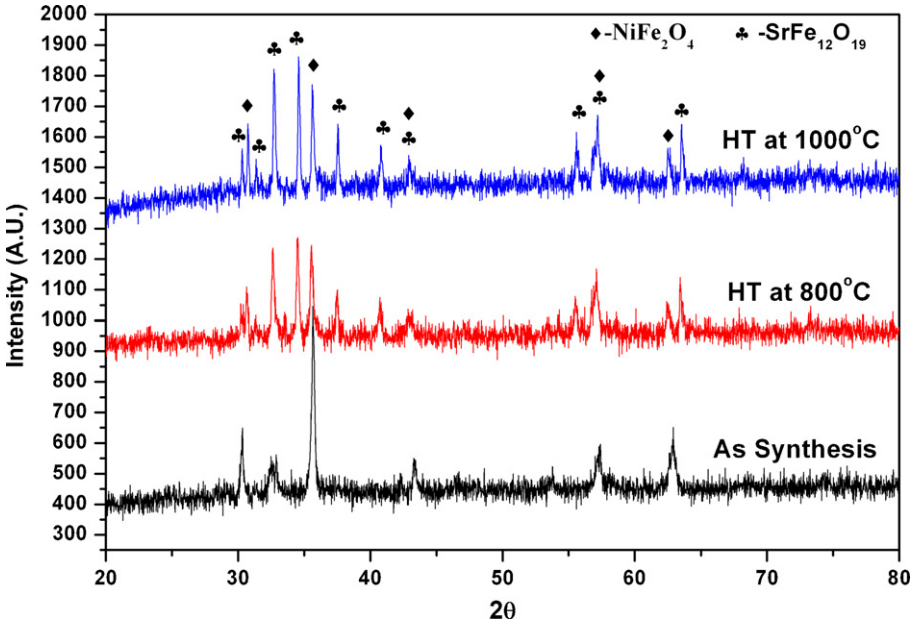

Fig. 3. XRD patterns of $SrFe_{12}O_{19}/NiFe_2O_4$ nanoparticles in 'as synthesized' and heat treated at 800 and1000 °C in nitrogen atmosphere.

in Fig. 3. From the results, it can be inferred that the ferrite powder in 'as-synthesized' condition is showing only the peak corresponding to $NiFe_2O_4$, $2\theta = 35.710^\circ$ (JCPDS No. 3-875). When annealed at 800?C, the peak corresponding to $SrFe_{12}O_{19}$, $2\theta = 34.386^\circ$ (JCPDS No. 24-1207) phase is also observed. As expected, the degree of crystallinity and amount of $SrFe_{12}O_{19}/NiFe_2O_4$ nanoparticles is further increased by increasing the heat treatment temperature from 800 to 1000 °C. By comparing the area under the peak corresponding the $SrFe_{12}O_{19}$ ($2\theta = 34.386^\circ$) and $NiFe_2O_4$ ($2\theta = 35.710^\circ$) phases, it is observed that $NiFe_2O_4$ is about 80% of $SrFe_{12}O_{19}$ for the powder heat treated at 1000 °C. The crystallite size of $SrFe_{12}O_{19}$ (Fig. 3) phase ($2\theta = 34.386^\circ$) is found to increase with increase in heat treatment temperature. It increases from 45 nm at 800 °C to 55 nm at 1000 °C.

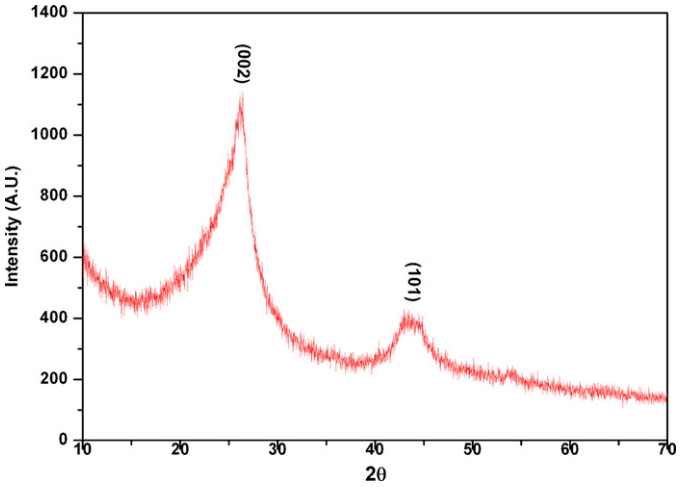

Fig. 4. The XRD pattern of CNTs synthesis by the catalytic decomposition of acetylene gas in the temperature range of 750–800 °C.

The XRD pattern of CNTs ((JCPDS 01-0640) synthesis by the catalytic decomposition of acetylene gas in the temperature range of 750–800 °C is shown in Fig. 4. The interlayer spacing corresponding to the plane (0 0 2) is found to be 3.40 Å. This is observed to be slightly higher than that of pure graphite (3.35 Å). The increase in d spacing is perhaps due to the influence of the nature of Fe catalyst used in the present study. Peak corresponding to (0 0 2) plane (Fig. 4) is quite broad, indicating that the graphitization is low. From XRD study, it is found that soft ferrite phase ($NiFe_2O_4$) is crystallized in the 'as synthesized' condition which was not obtained for 'as synthesized' powder prepared by co-precipitation method [17]. In low combustion synthesis method, strontium hexaferrite phase is obtained at relatively low temperature (800 °C) than for powder heat treated after co-precipitation synthesis [3,17].

The FESEM micrographs of 'as synthesized' and heat treated ferrite powders at temperatures of 800 and 1000 °C are shown in Fig. 5. In the 'as-synthesized' condition, the particles seem to have spherical shaped morphology with particle size in the range of 15–20 nm (Fig. 5a). With increasing heat treatment temperature, the particles grow and constitute multiple morphologies (Fig. 5b and c). This process of crystal growth and morphological evolution can be described in terms of Ostwald ripening. As the HT temperature is increased, small size nanoparticles slowly disappear except for the few that grow larger, at the expense of smaller ones. Thus particles of small size act as nutrients for the bigger ones. At 1000 °C, $SrFe_{12}O_{19}/NiFe_2O_4$ nanoparticles (with size in the range of 85–100 nm) having hexagonal plate and pyramidal shapes are observed (Fig. 5c). This is also evidenced by TEM micrograph of the powder in 'as-synthesized' and heat treated condition (Fig. 6). These multiple morphologies, possessing large surface areas,

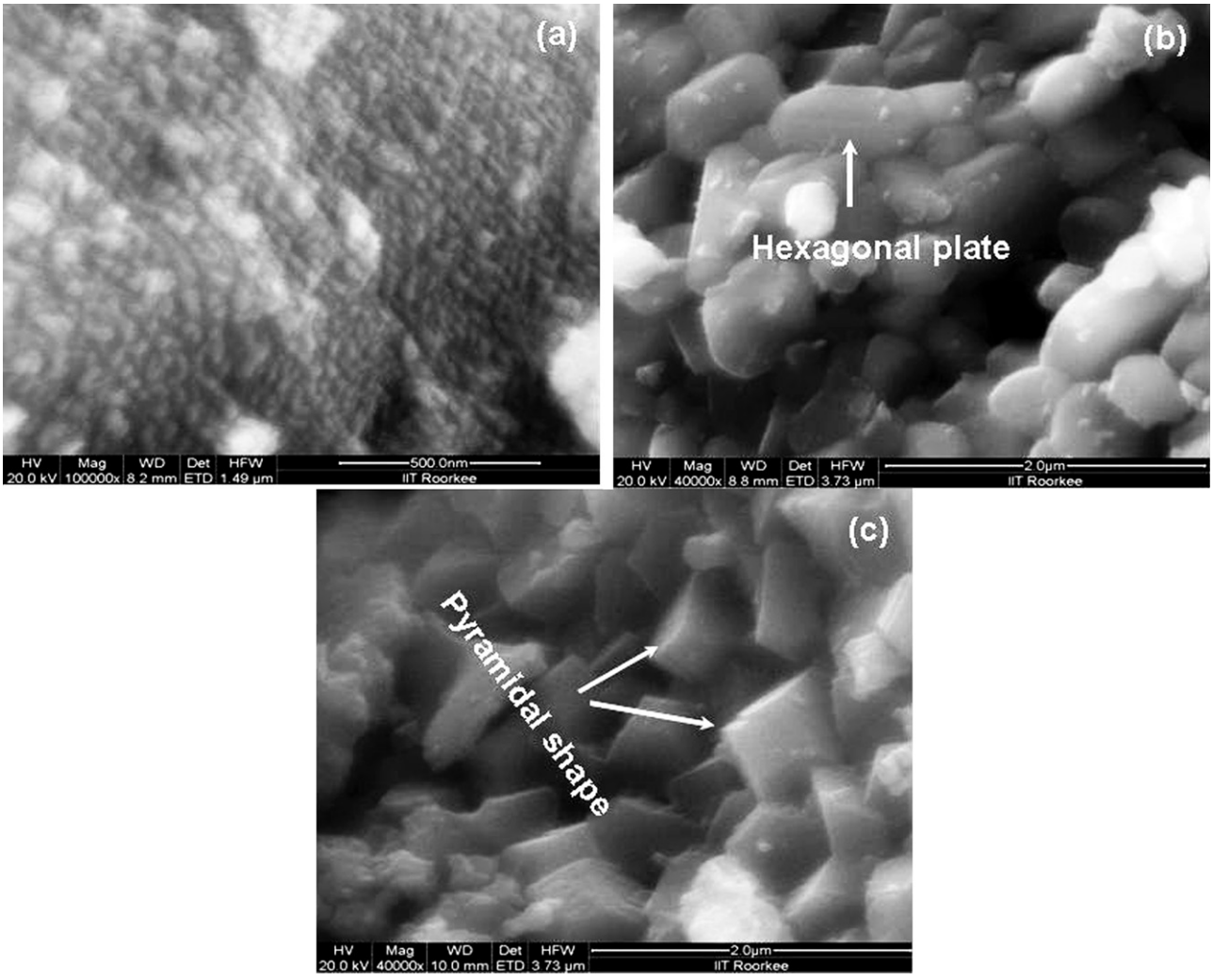

Fig. 5. FESEM micrographs showing the effect of heat treatment temperature on the morphology of $SrFe_{12}O_{19}/NiFe_2O_4$ nanoparticles, (a) 'as synthesized' and heat treated at (b) 800 °C and (c) 1000 °C in nitrogen atmosphere.

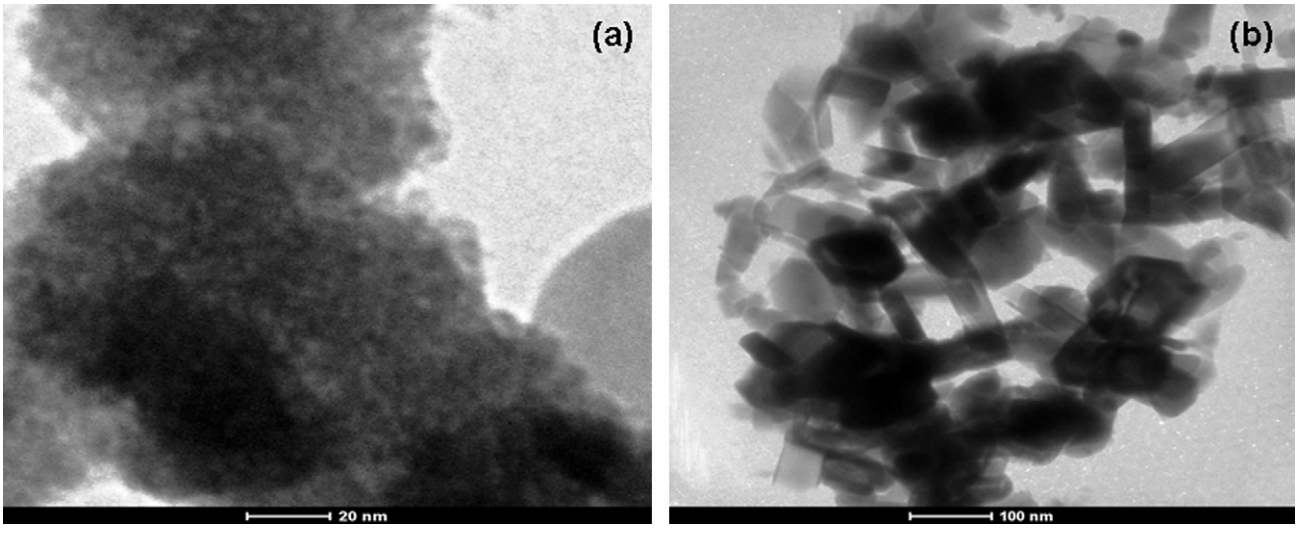

Fig. 6. TEM micrographs showing the effect of heat treatment temperature on the morphology of $SrFe_{12}O_{19}/NiFe_2O_4$ nanoparticles, (a) 'as synthesized' and (b) heat treated at 1000 °C in nitrogen atmosphere.

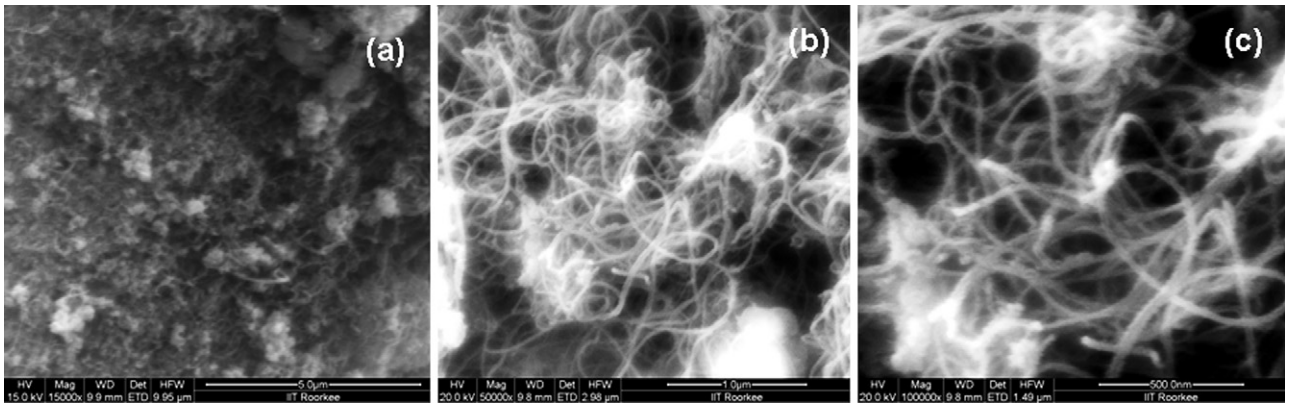

Fig. 7. FESEM micrographs showing the growth of CNTs synthesis by the catalytic decomposition of acetylene gas in the temperature range of 750–800 °C.

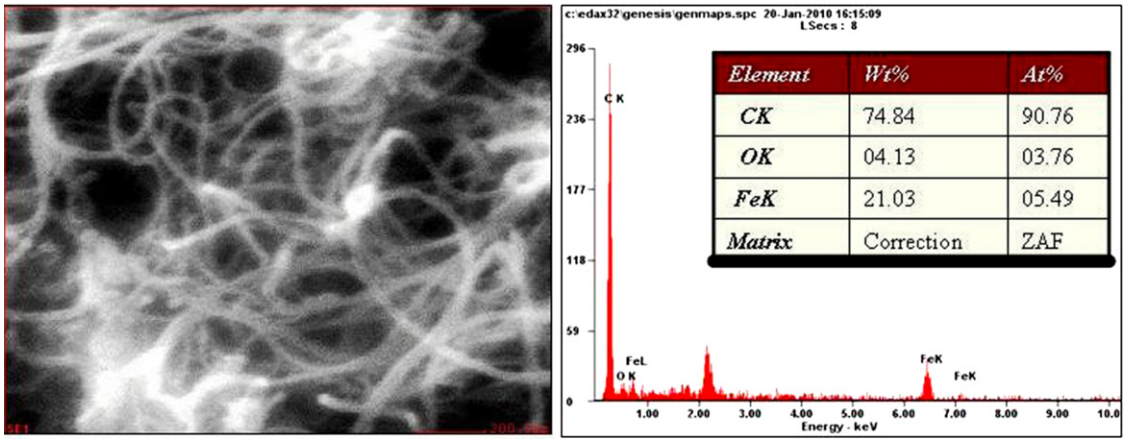

Fig. 8. FESEM micrographs with EDAX of CNTs synthesis by the catalytic decomposition of acetylene gas in the temperature range of 750–800 °C.

will lead to plenty of interfacial polarization to weaken the energy of EM waves. It is reported that Barium and strontium hexaferrite nanoparticles with hexagonal pyramidal and hexagonal plate like morphologies are potential materials for the RADAR absorption applications [2,3,13,17,30]. Fig. 7 shows the typical FESEM of the top view of the CNTs arrays grown over Fe-catalyst. The higher magnification shows long and thin multiwalled carbon nano tubes with diameter in the range of 30–40 nm. The quality of CNTs was confirmed by EDAX analysis where peaks corresponding to iron (catalyst) and oxygen are also observed along with carbon (Fig. 8).

The magnetic measurements of $SrFe_{12}O_{19}/NiFe_2O_4$ nanoparticles have low coercivity (242.752 G) and low remanance values (5.810 emu/g) in the 'as synthesized' condition (Fig. 9). This confirms the formation of soft magnetic phase ($NiFe_2O_4$) in the 'as synthesized' condition which is also confirmed by XRD pattern (Fig. 3) of 'as synthesized' powder. But when the 'as synthesized' powders are heat treated at 800 and 1000 °C in nitrogen atmosphere for 4 h, the particles appear to transform from soft magnetic to mixture of soft and hard magnetic ($SrFe_{12}O_{19}/NiFe_2O_4$) phases (Fig. 3). Saturation magnetization is found to be dependent on HT temperature. It increases from 27.443 to 63.706 emu/g with increase in HT temperature (Fig. 9). The rise in saturation magnetization with the HT temperature is attributed to the increased formation of $SrFe_{12}O_{19}/NiFe_2O_4$ ferrites which is confirmed by X-ray pattern of powder HT at 1000 °C (Fig. 3) [17,31]. The coercivity of 1793 G is observed for the powder heat treated at 800 °C and thereafter increases to 2639 G at 1000 °C. This might be due to the increased formation of strontium

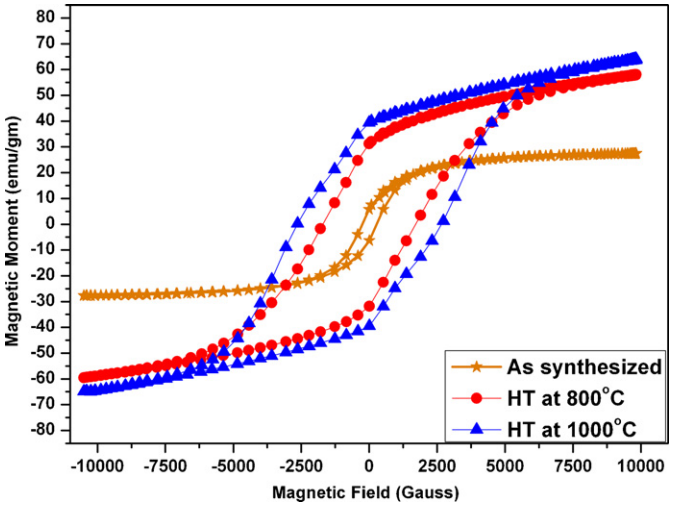

Fig. 9. The effect of HT temperature on hysteresis loops of $SrFe_{12}O_{19}/NiFe_2O_4$ nanoparticles in 'as synthesized' condition and heat treated at 800 and 1000 °C in nitrogen atmosphere.

Table 1
Showing the effect of heat treatment temperature on the morphology and magnetic parameters of $SrFe_{12}O_{19}/NiFe_2O_4$ nanoparticles.

Temperature (°C)	Morphology	Coercivity (Gauss)	Remanance. Mr (emu/g)	Saturation magnet isatio n Ms (emu/g)	Mr/Ms
80 (As synthesized)	Spherical (15–20 nm)	242.752	5.810	27.443	0.211
800	Small hexagonal (80–90 nm)	1793	32.104	57.811	0.555
1000	Large hexagonal and pyramid (85–100 mn)	2639	39.425	63.706	0.618

hexaferrite with increase in HT temperature which has a high intrinsic coercive force [3,17]. Furthermore, the change in morphology and particle size affects the magnetic properties [17,31]. Thus the synthesis of spinel $NiFe_2O_4$ along with hexagonal $SrFe_{12}O_{19}$ particles in nano size range results in higher saturation magnetization than those reported for single phase strontium hexaferrite, nickel ferrite and strontium/nickel/zinc ferrite nanoparticles [3,6,7,17,31]. Hexaferrite nanoparticles having high saturation magnetization find their applications in magnetic recordings in hard disks, floppy disks, video tapes, etc. [32]. The effect of HT temperatures on the morphology and magnetic parameters is shown in Table 1.

Complex permittivity and permeability values represent the dielectric and magnetic properties of magnetic materials. The real parts (ε', μ') of complex permittivity and permeability symbolize the storage capability of electric and magnetic energy. The imaginary parts (ε'', μ'') represent the loss of electric and magnetic energy. As a microwave absorber, large imaginary parts of complex permittivity and permeability are expected. The real and imaginary parts of complex permittivity (Fig. 10a and b) and permeability (Fig. 11a and b) of $SrFe_{12}O_{19}/NiFe_2O_4$ nanoparticles are plotted as a function of frequency in X-band (8.2–12 GHz). It is observed that with the increase in heat treatment temperature from 'as synthesized' condition to 1000 °C, both complex permittivity and permeability are observed to increase continuously. The real part of permittivity is found to increase from 5.618 (average value) in 'as synthesized' condition to 9.018 (average value) when heat treated at 1000 °C (Fig. 10a). The same trend is observed for the imaginary part of permittivity. The maximum imaginary permittivity of 2.645 (average value) is observed for the material heat treated at 1000 °C (Fig. 10b). Also, the real permeability increases from 1.171 (average value) in 'as synthesized' condition to 1.263 (average value) when heat treated at 1000 °C (Fig. 11a). Similarly imaginary permeability is also increasing with increase in heat treatment temperature. The maximum imaginary permeability of 2.039 (average value) is observed for the powder heat treated at 1000 °C (Fig. 11b). The increase in complex permittivity and permeability with increase in heat treatment temperature in all the cases is attributed to the increased formation and crystallization of strontium hexaferrite and nickel ferrite nanoparticles with increase in HT temperature [17]. The significance of the results is the stability in the values of complex permittivity and permeability (obtained for large bandwidth) than those reported in literature [3,6,7] for pure strontium hexaferrite and nickel ferrite. The real and imaginary parts of complex permittivity (Fig. 12a and b) and permeability (Fig. 13a and b) of $SrFe_{12}O_{19}/NiFe_2O_4$/CNTs (ferrite/CNTs) composite are plotted as a function of frequency in X-band. The real part of permitivity of

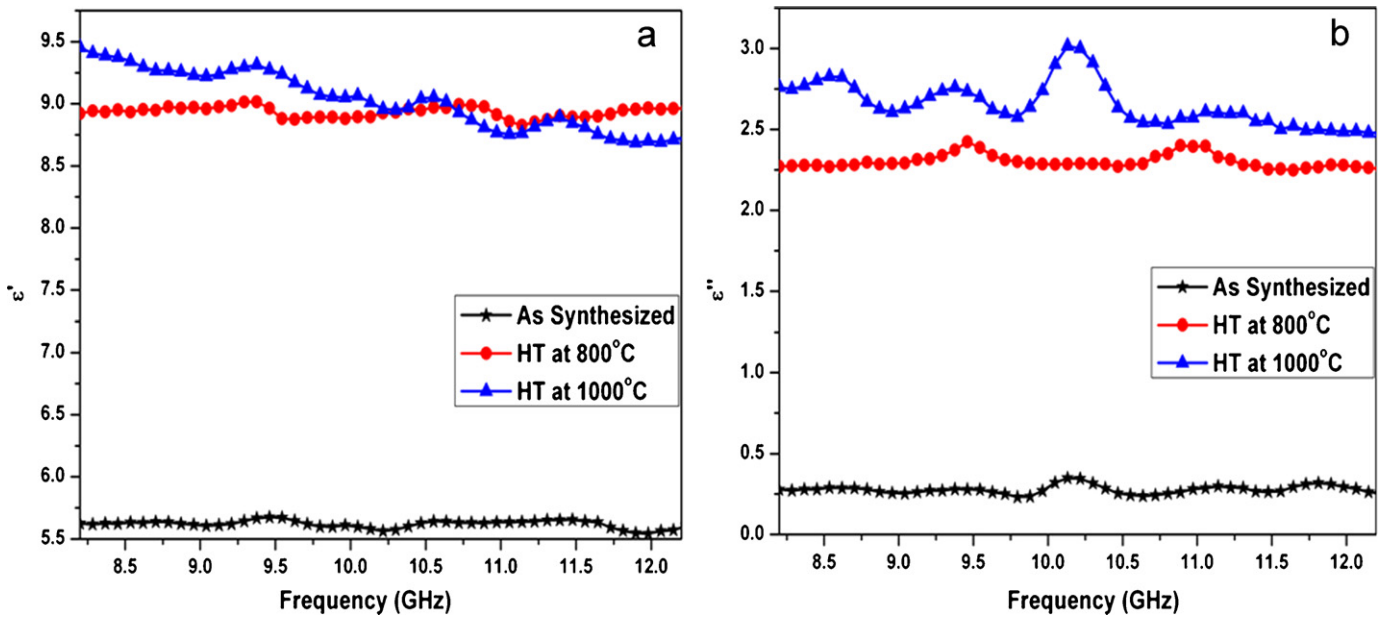

Fig. 10. The effect of HT temperature on real (ε') and imaginary (ε'') part of permitivity of $SrFe_{12}O_{19}/NiFe_2O_4$ nanoparticles in 'as synthesized' condition and heat treated at 800 and 1000 °C in nitrogen atmosphere.

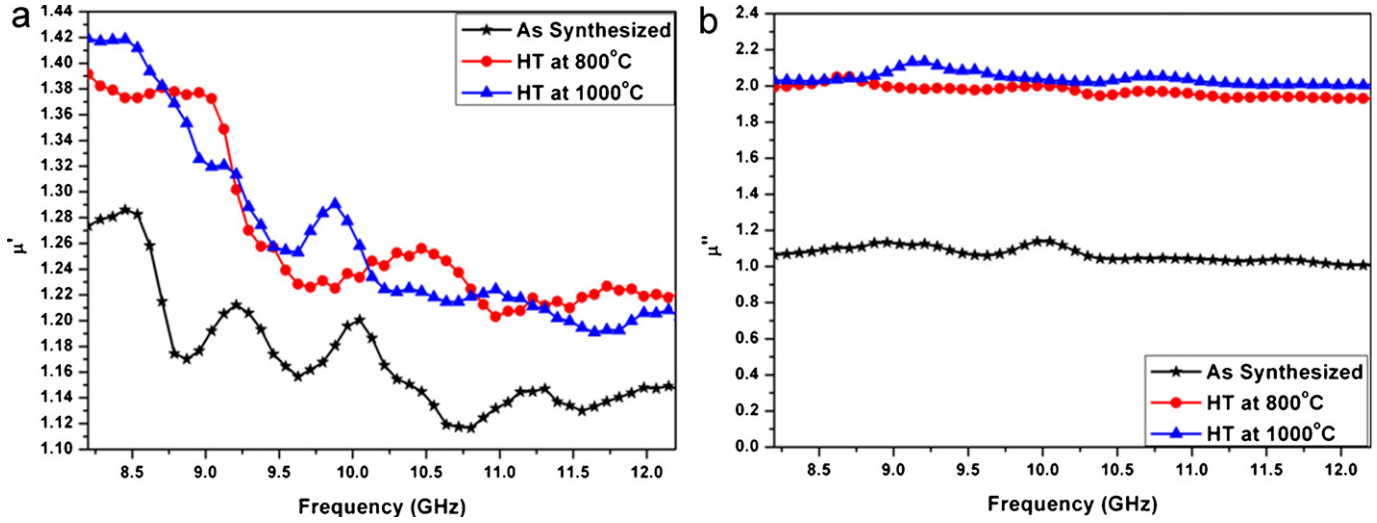

Fig. 11. The effect of HT temperature on real (μ') and imaginary (μ'') part of permeability of $SrFe_{12}O_{19}/NiFe_2O_4$ nanoparticles in 'as synthesized' condition and heat treated at 800 and 1000 °C in nitrogen atmosphere.

ferrite/CNTs increases with increase in amount of CNTs (wt%). It increases from 9.873 (average value) for the ferrite/CNTs composite containing 5% of CNTs and 75% ferrite to 17.723 (average value) for the ferrite/CNTs composite containing 20% of CNTs and 60% ferrite (Fig. 12a). The similar trend is observed for the imaginary part of permittivity. The maximum imaginary permittivity of 5.913 (average value) is observed for ferrite/CNTs composite containing 20% of CNTs and 60% ferrite (Fig. 12b). The increase in real and imaginary part of permittivity of ferrite/CNTs composite with increase in wt% of CNTs might be due to the high value of complex permittivity (real and imaginary both) of CNTs which is also measured for pure CNTs (Fig. 12a and b). Also, the real part permeability of ferrite/CNTs decreases with increase in amount of CNTs (wt%). It decreases from 1.264 (average value) for the ferrite/CNTs composite containing 5% of CNTs and 75% ferrite to 1.248 (average value) for the ferrite/CNTs composite containing 20% of CNTs and 60% ferrite (Fig. 13a). The same trend is observed for the imaginary part of permeability. The maximum imaginary permeability of 1.746 (average value) is observed for ferrite/CNTs composite containing 5% of CNTs and 75% ferrite (Fig. 13b). The decrease in real and imaginary part of permeability of ferrite/CNTs composite with increase in wt% of CNTs might be due to the low value of complex permeability (real and imaginary both) of CNTs which is also measured for pure CNTs (Fig. 13a and b).

The reflection losses (RL) for 'as synthesized' $SrFe_{12}O_{19}/NiFe_2O_4$ nanoparticles are low for all the frequencies ranging 8.2–12.2 GHz (Fig. 14). The minimum and maximum values of RL are −3.710 and −14.122 dB at 12.2 and 9.039 GHz respectively. For $SrFe_{12}O_{19}/NiFe_2O_4$ nanoparticles heat treated at 800 °C, the reflection loss is evidently improved to

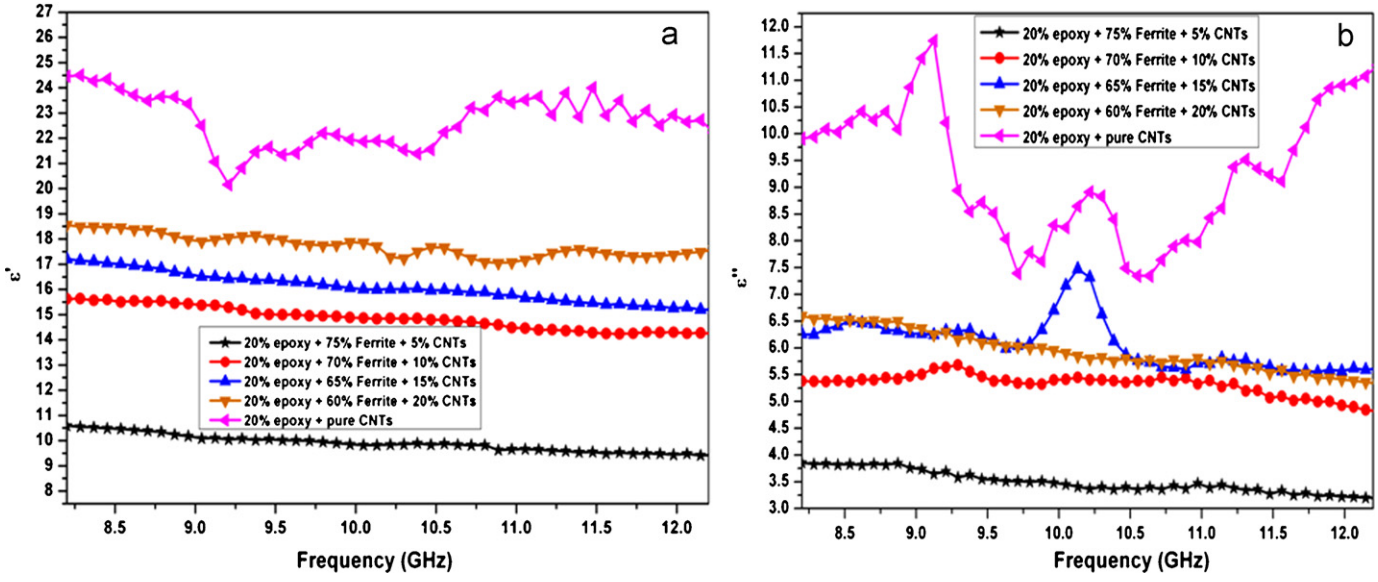

Fig. 12. The effect of addition of CNTs on real (ε') and imaginary (ε'') part of permitivity of $SrFe_{12}O_{19}/NiFe_2O_4$ nanoparticles.

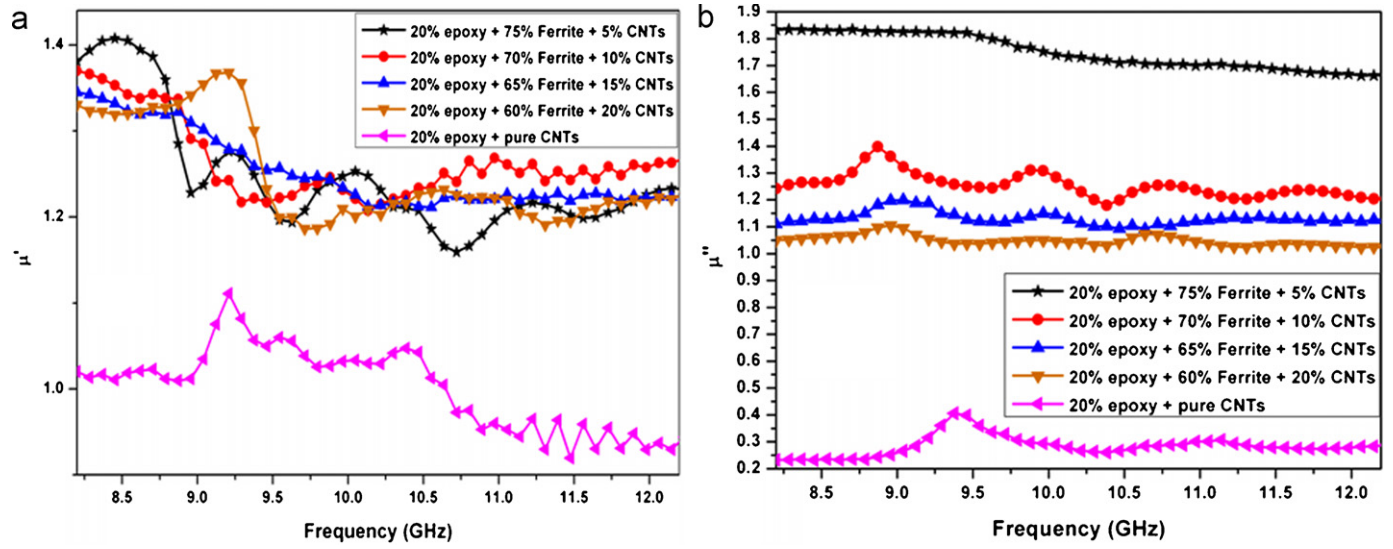

Fig. 13. The effect of addition of CNTs on real (μ') and imaginary (μ'') part of permeability of $SrFe_{12}O_{19}/NiFe_2O_4$ nanoparticles.

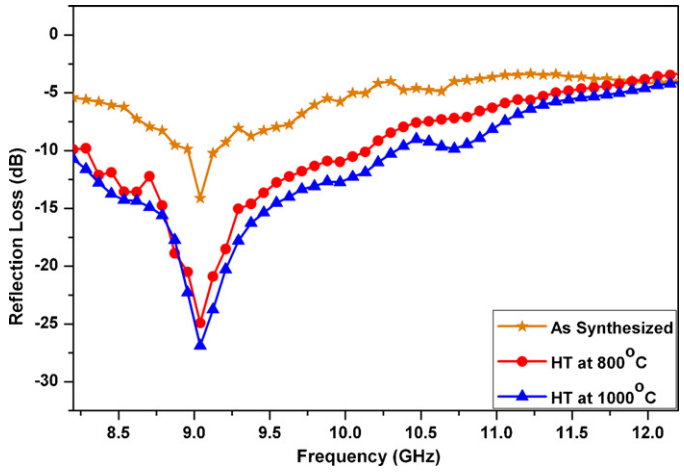

Fig. 14. The effect of HT temperature on reflection loss of $SrFe_{12}O_{19}/NiFe_2O_4$ in 'as synthesized' condition and heat treated at 800 and 1000 °C.

−24.826 dB at 9.039 GHz and has further enhanced to −26.984 dB for the material heat treated at 1000 °C (Fig. 14). The increment in reflection loss with increasing heat treatment temperature is attributed to the increased formation and crystallization (Fig. 3) of $SrFe_{12}O_{19}/NiFe_2O_4$ nanoparticles (crystallization effect) [17]. The strongest reflection loss and the widest bandwidths (for RL >10 dB) are given in Table 2. The improvement of reflection loss originated from the formation of hard and soft ferrite which can be explained on the basis of exchange coupling interaction between hard magnetic ($SrFe_{12}O_{19}$) and soft magnetic ($NiFe_2O_4$) phases, which changes the relative complex permeability of the materials. In this study, the nanocomposite powders are synthesized by low combustion method so that two kinds of grains can be combined. The composite powder including hexaferrite ($SrFe_{12}O_{19}$) and spinel ferrite ($NiFe_2O_4$) coupled to each other by exchange through interface of ferrite particles. There will be more interfaces if the grain size is smaller, and there will be stronger exchange coupling interaction at the interface. As we know, the cubic spinel crystal structure of $NiFe_2O_4$ is similar to the structure of S-block of $SrFe_{12}O_{19}$, so it is possible that the vacancy of $NiFe_2O_4$ is combined with Fe^{3+} at the $SrFe_{12}O_{19}$ surface, which is another possible reason for strong interface coupling interaction. Thus, exchange coupling interaction existing between hard and soft magnetic phases improves the dielectric and microwave absorption properties (interface effect) which are in agreement with the present study [12,14,17]. The size of particles heat-treated at 1000 °C (85–100 nm) is larger than that of particles heat-treated at 800 °C (80–90 nm). However, the strongest RL at 9.039 GHz for HT 1000 °C sample is −26.984 dB, which is larger than RL for HT at 800 °C (−24.826 dB). Obviously, there is a competition between interface effect and the crystallization effect on the reflection loss.

The microwave absorption performances of thus-prepared ferrite/CNTs composite at the microwave frequency of 8.2–12.2 GHz range were also measured (Fig. 15). For comparison, the microwave absorption properties of pure CNTs and pure

Table 2
Showing the strongest reflection loss and the widest bandwidths (for RL > 10 dB) in 'as synthesized' and heat treated conditions.

Powder	RL (dB) at 8.2 GHz	RL(dB) at 12.2 GHz	The widest bandwidth for RL >10 dB (in GHz)	The strongest RL (dB) at 9.039 GHz
As synthesized	−5.404	−3.710	0.16 (9.04–9.20)	−14.122
HT at 800°C	−9.902	−3.262	1.93 (8.28–10.21)	−24.826
HT at 1000 °C	−10.730	−4.020	2.10 (8.20–10.30)	−26.984

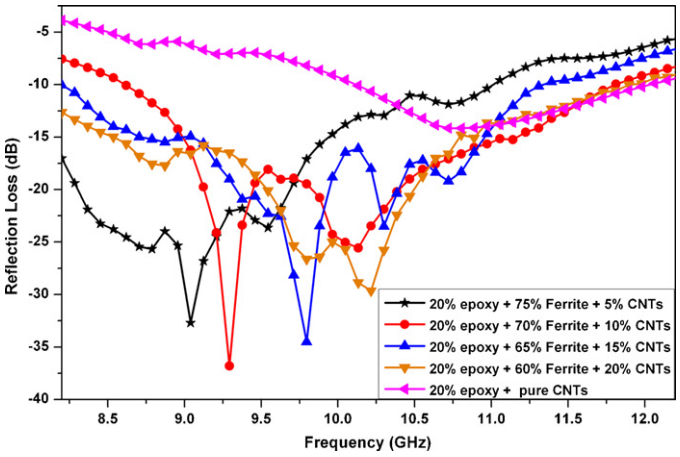

Fig. 15. The effect of addition of CNTs on reflection loss of $SrFe_{12}O_{19}/NiFe_2O_4$ nanoparticles.

$SrFe_{12}O_{19}/NiFe_2O_4$ powder (without CNTs) were also studied (Figs. 14 and 15). It showed that the $SrFe_{12}O_{19}/NiFe_2O_4$ with CNTs composite exhibited superior microwave absorption to that of pure $SrFe_{12}O_{19}/NiFe_2O_4$ and pure CNTs. The maximum reflection loss reaches to −36.81 dB at 9.292 GHz and −10 dB bandwidth reaches 3.27 GHz for the composite containing 10% of CNTs, 70% ferrite and 20% epoxy. The result also showed that (Fig. 15) the positions of microwave absorption peaks moved towards the higher frequencies by increasing the amount of CNTs into $SrFe_{12}O_{19}/NiFe_2O_4$ nanoparticles. This indicates that the absorption peak frequency of the ferrite/CNTs composites can be manipulated easily by changing the amount of CNTs and $SrFe_{12}O_{19}/NiFe_2O_4$ nanoparticles. Generally excellent electromagnetic wave absorption is resulted from the efficient complement between the relative permittivity and the permeability of materials. Either only the magnetic loss or only the dielectric loss may induce a weak electromagnetic wave absorption property due to the imbalance of the electromagnetic match [33]. For the pure CNTs, only dielectric loss (complex permitivity) contributed to the electromagnetic loss, while for the $SrFe_{12}O_{19}/NiFe_2O_4$, the effect of magnetic loss was dominant over the dielectric loss. It means that the magnetic loss and the dielectric loss were out of balance in both the cases, which resulted in less electromagnetic wave absorption. The improved microwave absorption of the $SrFe_{12}O_{19}/NiFe_2O_4$ with mixed CNTs composite obviously originated from the combination of the diamagnetic CNTs and ferromagnetic $SrFe_{12}O_{19}/NiFe_2O_4$ nanoparticles, which had better match of the dielectric loss and magnetic loss [33]. The typical ferromagnetic property of $SrFe_{12}O_{19}/NiFe_2O_4$ composite was considered beneficial for the increase of the magnetic loss capability [34]. Similar phenomena were also reported in the cases of $CoFe_2O_4$ and CNTs composite [35]. The −10 dB absorption bandwidth corresponds to 68% EM wave amplitude attenuation or 90% power attenuation, whereas a −20 dB absorption bandwidth corresponds to 90% amplitude attenuation or 99% power attenuation [11]. The epoxy resin is an insulator and nonmagnetic; thus, it is transparent to EM waves. In the $SrFe_{12}O_{19}/NiFe_2O_4$ composite, the epoxy resin only functions as a matrix [11]. The reflection loss of the composite mainly stems from the contribution of $SrFe_{12}O_{19}/NiFe_2O_4$ and CNTs composite. Thus more than 99% power attenuation is observed for the composite containing 10% of CNTs, 70% ferrite and 20% epoxy which suits its application in Stealth defense in all military platforms.

5. Conclusions

(1) The hexagonal plate and pyramid shaped (85–100 nm) $SrFe_{12}O_{19}/NiFe_2O_4$ nanoparticles are successfully synthesized for the powder heat treated at 1000 °C.
(2) The $SrFe_{12}O_{19}/NiFe_2O_4$ nanoparticles show high value of saturation magnetization (63.706 emu/g) and intrinsic coercivity (2639 G) when heat treated at 1000 °C as compared to powder heat treated at 800 °C (57.811 emu/g, 1793 G respectively).
(3) The real and imaginary parts of permittivity and permeability increases with increase in heat treatment temperature. The maximum reflection loss of −29.62 dB (99% power attenuation) at 10.21 GHz is obtained for the material heat treated at 1000 °C.
(4) Addition of certain mass of CNTs improves the microwave absorption properties and wave band of $SrFe_{12}O_{19}/NiFe_2O_4$ absorbent. When 10 wt% CNT is mixed with hexaferrite to fabricate a composite with 2 mm thickness, the maximum reflection loss reaches to −36.817 dB at 9.292 GHz and −10 dB bandwidth reaches 3.27 GHz.

Acknowledgment

The authors acknowledge Ministry of Human Resource Development (MHRD), Government of India for the fellowship granted to the first author of this study.

References

[1] D.S. Li, T. Horikawa, J.R. Liu, M. Itoh, K. Machida, Electromagnetic wave absorption properties of iron/rare earth oxide composites dispersed by amorphous carbon powder, J. Alloys Compd. 408 (2006) 1429–1433.
[2] R. Sharma, R.C. Agarwala, V. Agarwala, Development of radar absorbing nano crystals under thermal irradiation, J. Nanopart. Res. 2 (2008) 91–104.
[3] S. Tyagi, R.C. Agarwala, V. Agarwala, Microwave absorption and magnetic studies of strontium hexaferrite nanoparticles synthesized by modified flux method, J. Nanopart. Res. 10 (2010) 19–27.
[4] A. Ghasemi, A. Morisako, Structural and electromagnetic characteristics of substituted strontium hexaferrite nanoparticles, J. Magn. Magn. Mater. 320 (2008) 1167–1172.
[5] P. Singh, V.K. Babbar, A. Razdan, S.L. Srivastava, R.K. Puri, Complex permeability and permittivity, and microwave absorption studies of $Ca(CoTi)_xFe_{12-2x}O_{19}$ hexaferrite composites in X-band microwave frequencies, Mater. Sci. Eng. B 67 (1999) 132–138.
[6] V. Sunny, P. Kurian, P. Mohanan, P.A. Joy, M.R. Anantharaman, A fexible microwave absorber based on nickel ferrite nanocomposite, J. Alloys Compd. 489 (2010) 297–303.
[7] C.H. Peng, C.C. Hwang, J. Wan, J.S. Tsai, S.Y. Chen, Microwave-absorbing characteristics for the composites of thermal-plastic polyurethane (TPU)-bonded NiZn-ferrites prepared by combustion synthesis method, Mater. Sci. Eng. B 117 (2005) 27–36.
[8] P.C. Fannin, C.N. Marin, I. Malaescu, N. Stefu, P. Vlazan, S. Novaconi, P. Sfirloaga, S. Popescu, C. Couper, Microwave absorbent properties of

nanosized cobalt ferrite powders prepared by coprecipitation and subjected to different thermal treatments, Mater. Des. 32 (2011) 1600–1604.
[9] D.A. Makeiff, Trisha Huber, Microwave absorption by polyaniline–carbon nanotube composites, Synth. Met. 156 (2006) 497–505.
[10] J.B. Kim, S.K. Lee, C.G. Kim, Comparison study on the effect of carbon nano materials for single-layer microwave absorbers in X-band, Compos. Sci. Technol. 68 (2008) 2909–2916.
[11] X. Liu, Z. Zhang, Y. Wu, Absorption properties of carbon black/silicon carbide microwave absorbers, Composite: Part B 42 (2011) 326–329.
[12] T. Maeda, S. Sugimoto, T. Kagotani, N. Tezuka, K. Inomata, Effect of soft/hard exchange interaction on natural resonance frequency and electromagnetic wave absorption of the rare earth–iron–boron compounds, J. Magn. Magn. Mater. 281 (2004) 195–205.
[13] R. Sharma, R.C. Agarwala, V. Agarwala, Development of electroless (Ni–P)/$BaNi_{0.4}Ti_{0.4}Fe_{11.2}O_{19}$ nanocomposite powder for enhanced microwave absorption, J. Alloys Compd. 467 (2009) 357–365.
[14] J.R. Liu, M. Itoh, K.I. Machida, Magnetic and electromagnetic wave absorption properties of alpha-Fe/Z-type Ba-ferrite nanocomposites, Appl. Phys. Lett. 88 (2006), 062503/1–3.
[15] Z. Zheng, B. Xu, L. Huang, L. He, X. Ni, Novel composite of Co/carbon nanotubes: synthesis, magnetism and microwave absorption properties, Solid State Sci. 10 (2008) 316–320.
[16] H. Li, J. Wanga, Y. Huanga, X. Yana, J. Qia, J. Liub, Y. Zhanga, Microwave absorption properties of carbon nanotubes and tetrapod-shaped ZnO nanostructures composites, materials, Mater. Sci. Eng. B 175 (2010) 81–85.
[17] S. Tyagi, H. B.Baskey, R. C. Agarwala, V., Agarwala, T. C. Shami, Development of hard/soft ferrite nanocomposite for enhanced microwave absorption, Ceram. Int., in press
[18] D.L. Jhao, H.S. Zhao, W.C. Zhou, Dielectric properties of nano Si/C/Ncomposite powder and nano SiC powder at high frequencies, Physica E 9 (2001) 679–685.
[19] H.O. Jung, S.O. Kyung, G.K. Chun, S.H. Chang, Design of radar absorbing structures using glass/epoxy composite containing carbon black in X-band frequency ranges, Compos. Part B: Eng. 35 (2004) 49–56.
[20] S. Sugimoto, T. Maeda, D. Book, T. Kagotani, K. Inomata, M. Homma, H. Ota, Y. Houjou, R. Sato, GHz microwave absorption of a fine α-Fe structure produced by the disproportionation of Sm_2 Fe_{17} in hydrogen, J. Alloys Compd. 330–332 (2002) 301–306.
[21] B. Vishwanathan, V.R.K. Murthy, Ferrite Materials Science and Technology, Narosa Publishing House, New Delhi, 1990.
[22] B.D. Cullity, C.D. Graham, Introduction to Magnetic Materials, 2nd ed., John Wiley & Sons, New Jersey, 2008.
[23] T.S. Chin, S.L. Hsu, M.C. Deng, Barium ferrite particulates prepared by salt-melt method, J. Magn. Magn. Mater. 120 (1993) 64–68.
[24] X. Liu, J. Wang, L.M. Gan, S.C. Ng, Improving the magnetic properties of hydrothermally synthesized barium ferrite, J. Magn. Magn. Mater. 195 (1999) 452–459.
[25] M. Sivakumar, A. Gedanken, W. Zhong, Y.W. Du, D. Bhattacharya, Y. Yeshurun, I. Felner, Nanophase formation of strontium hexaferrite fine powder by sonochemical method using $Fe(CO)_5$, J. Magn. Magn. Mater. 268 (2004) 95–104.
[26] J. Huang, H. Zhuang, W. Li, Optimization of the microstructure of low temperature combustion synthesized barium ferrite powder, J. Magn. Magn. Mater. 256 (2003) 390–395.
[27] M. O'Donoghue, A Guide to Man-made Gemstones, Van Nostrand Reinhold, Great Britain, 1983, pp. 40–44.
[28] K.S. Suslick, Ultrasound its chemical, Physical and Biological Effects, VCH, Weinheim, 1988.
[29] K.B.K. Teo, C. Singh, M. Chowalla, W.I. Milne, H.S. in:, Nalwa, Catalytic synthesis of carbon nanotubes and nanofibers, Encyclopedia Nanosci. Technol. 1 (2004) 665.
[30] R. Sharma, R.C. Agarwala, V. Agarwala, Development of RADAR absorbing nano crystals by microwave irradiation, Mater. Lett. 62 (2008) 2233–2236.
[31] M.M. Hessien, M.M. Rashad, K. El-Barawy, Controlling the composition and magnetic properties of strontium hexaferrite synthesized by co-precipitation method, J. Magn. Magn. Mater. 320 (2008) 336–343.
[32] Y.P. Fu, C.H. Lin, Fe/Sr Ratio effect on magnetic properties of strontium ferrite powders synthesized by microwave induced combustion process, J. Alloys Compd. 386 (2005) 222–227.
[33] A. Wadhawan, D. Garrett, J.M. Perez, Nanoparticle-assisted microwave absorption by single-wall carbon nanotubes, Appl. Phys. Lett. 83 (2003) 2683.
[34] X.F. Zhang, X.L. Dong, H. Huang, Y.Y. Liu, W.N. Wang, X.G. Zhu, B. Lv, J.P. Lei, C.G. Lee, Microwave absorption properties of the carbon-coated nickel nanocapsules, Appl. Phys. Lett. 89 (2006) 053115.
[35] R.C. Che, C.Y. Zhi, C.Y. Liang, X.G. Zhou, Fabrication, microwave absorption of carbon nanotubes/$CoFe_2O_4$ spinel nanocomposite, Appl. Phys. Lett. 88 (2006) 033105.